



ELSEVIER

Biophysical Chemistry 72 (1998) 101–109

Biophysical  
Chemistry

## Calcium waves and oscillations driven by an intercellular gradient of inositol (1,4,5)-trisphosphate

James Sneyd<sup>a,\*</sup>, Matthew Wilkins<sup>b,1</sup>, Andreja Strahonja<sup>c</sup>, Michael J. Sanderson<sup>c</sup>

<sup>a</sup>Department of Mathematics, University of Michigan, 2072 East Hall, 525 East University Avenue, Ann Arbor, MI, 48109–1109, USA

<sup>b</sup>Department of Mathematics and Statistics, University of Canterbury, Christchurch, New Zealand

<sup>c</sup>Department of Physiology, University of Massachusetts Medical Center, Worcester, Massachusetts, USA

Revision received 26 January 1998; accepted 13 February 1998

### Abstract

In response to a local mechanical stimulus, mixed glial cells initially exhibit a propagating intercellular  $\text{Ca}^{2+}$  wave. Subsequently, cells within a zone, at a specific distance from the stimulated cell, display asynchronous intracellular  $\text{Ca}^{2+}$  oscillations. The experimental hypothesis that the initial  $\text{Ca}^{2+}$  wave could be mediated by the passive diffusion of inositol (1,4,5)-trisphosphate ( $\text{IP}_3$ ) from the stimulated cell has been verified by model simulations. Further simulations with the same model also show that  $\text{Ca}^{2+}$  oscillations can only occur within model cells when the  $\text{IP}_3$  concentration is within a specific range. Thus, this passive diffusion model predicts (a) that the  $\text{IP}_3$  concentration gradient established in the cells following mechanical stimulation will initiate  $\text{Ca}^{2+}$  oscillations in cells in a specific zone along this gradient and (b) that different  $\text{Ca}^{2+}$  oscillatory patterns will occur within a specified oscillatory zone. Both of these predictions have been confirmed by experimental data. The failure of experimentally observed  $\text{Ca}^{2+}$  oscillations to approach synchrony or entrain indicates a low intercellular calcium permeability of about  $0.1 \mu\text{m/s}$ , and further suggests that  $\text{Ca}^{2+}$  does not appear to act as a significant messenger in the initiation of these intercellular  $\text{Ca}^{2+}$  waves or oscillations. In conclusion a passive diffusion of  $\text{IP}_3$ , but not  $\text{Ca}^{2+}$ , through gap junctions remains the preferred hypothesis for the mechanism underlying mechanically-stimulated intercellular calcium waves and  $\text{Ca}^{2+}$  oscillations. © 1998 Elsevier Science B.V. All rights reserved

**Keywords:** Calcium waves; Oscillations; Intercellular gradient

### 1. Introduction

A wide diversity of cell types can communicate with their neighbors by means of an intercellular cal-

cium ( $\text{Ca}^{2+}$ ) wave, i.e. the propagation of an increase in intracellular  $\text{Ca}^{2+}$  concentration from cell to cell [1,2]. Intercellular  $\text{Ca}^{2+}$  waves can be initiated by a focal mechanical, electrical, or hormonal stimulus, and by propagating to numerous adjacent cells, may serve to coordinate a global cellular response. For instance, mechanical stimulation of a single ciliated tracheal epithelial cell causes an intercellular  $\text{Ca}^{2+}$  wave that propagates to surrounding cells, inducing

\* Corresponding author. Fax: +1 734 7630937;

e-mail: jsneyd@math.lsa.umich.edu

<sup>1</sup> Present address: Courant Institute, New York University, New York, NY, USA.

an increase in ciliate beat frequency over an area much larger than that of a single cell.

Intercellular  $\text{Ca}^{2+}$  waves also propagate between different cell types.  $\text{Ca}^{2+}$  waves between airway epithelial and smooth muscle cells [3] may regulate airway caliber whereas  $\text{Ca}^{2+}$  waves propagating between glial and endothelial cells may influence the function of the blood-brain barrier [4]. Intercellular  $\text{Ca}^{2+}$  waves between glial and neurons suggest a role in information processing by neuronal networks [5–7].

In mixed glial cultures, a mechanically stimulated intercellular wave is followed by asynchronous intracellular  $\text{Ca}^{2+}$  oscillations, that are not transmitted between cells. Further, cells displaying such oscillations can still transmit an intercellular wave.

### 1.1. The $\text{IP}_3$ passive diffusion hypothesis

Over the past few years, a great deal of experimental evidence has accumulated supporting the hypothesis that mechanically-stimulated intercellular  $\text{Ca}^{2+}$  waves can result from the diffusion of inositol 1,4,5-trisphosphate ( $\text{IP}_3$ ) through gap junctions [2]. According to this hypothesis (illustrated in Fig. 1),  $\text{IP}_3$  is initially produced in a single cell in response to mechanical stimulation. This  $\text{IP}_3$  binds to  $\text{IP}_3$  receptors (IPR) on the endoplasmic reticulum (ER) to stimulate the release of  $\text{Ca}^{2+}$  into the cytoplasm. Although  $\text{Ca}^{2+}$  can move through gap junctions, a cellular  $\text{Ca}^{2+}$  wave is the cellular response to a diffusing bolus of  $\text{IP}_3$ , passing between cells via gap junctions [1,4].

It is important to emphasize that this diffusional hypothesis of wave propagation cannot fully account for the observed behavior of all  $\text{Ca}^{2+}$  waves. For example, the intercellular  $\text{Ca}^{2+}$  waves observed in liver lobules [8,9] in hippocampal slices [7], or the intracellular  $\text{Ca}^{2+}$  waves observed in *Xenopus* oocytes [10], propagate over large distances and cannot simply rely on the diffusion of a messenger from a single point or cell. In these cases, it is likely that a process of regeneration is required to actively propagate the wave. However, the identity of the messenger passing between cells may still be  $\text{IP}_3$ . Alternatively,  $\text{Ca}^{2+}$  waves may result from the diffusion or release of an extracellular messenger [11–13]. An analysis of these actively propagated intercellular waves is considered in a separate paper [14].

To evaluate quantitatively our experimental data describing mechanically-stimulated intercellular  $\text{Ca}^{2+}$  waves in epithelial or glial cultures, we constructed a mathematical model that simulates wave propagation [15]. As this model assumed that  $\text{IP}_3$  moved between cells by passive diffusion through gap junctions but that  $\text{Ca}^{2+}$  did not move between cells, we have called this model the  $\text{IP}_3$  passive diffusion hypothesis. Although the model is in excellent agreement with a wide range of experimental data, we have subjected it to a further series of tests. Firstly, we estimate an approximate value for the intercellular  $\text{Ca}^{2+}$  permeability and conclude that intercellular diffusion of  $\text{Ca}^{2+}$  makes no qualitative difference to  $\text{Ca}^{2+}$  wave propagation. Secondly, we verify that a diffusive gradient of  $\text{IP}_3$  is established between cells by examining the spatial distribution and temporal properties of  $\text{Ca}^{2+}$  oscillations induced by the propagation of a  $\text{Ca}^{2+}$  wave. A detailed description of the experimental results upon which this paper is based is presented by Strahonja and Sanderson (unpublished data).

## 2. The model

As the model has been presented in detail [15], we give only a brief description here. There are only minor changes from the previous presentation, mostly for the purposes of improvement and clarity. We assume that:

1. Mechanical stimulation initiates the production of  $\text{IP}_3$  only in the stimulated cell, and that this  $\text{IP}_3$  diffuses from cell to cell through gap junctions. As the  $\text{IP}_3$  diffuses through the cytoplasm, it binds to  $\text{IP}_3$  receptors on the ER to release  $\text{Ca}^{2+}$  from the ER.
2. The  $\text{Ca}^{2+}$  flux through the IPR is dependent on the cytoplasmic free  $\text{Ca}^{2+}$  concentration. In combination with  $\text{IP}_3$ ,  $\text{Ca}^{2+}$  initially enhances  $\text{Ca}^{2+}$  release, but subsequently, slowly inactivates  $\text{Ca}^{2+}$  release. Thus  $\text{Ca}^{2+}$  release occurs in an autocatalytic fashion through the IPR, a process called  $\text{Ca}^{2+}$ -induced  $\text{Ca}^{2+}$  release, or CICR.
3. The flux of  $\text{IP}_3$  through gap junctions is proportional to its concentration difference across the gap junction; similarly for  $\text{Ca}^{2+}$ .

4. IP<sub>3</sub> is degraded with saturable kinetics, and the Ca<sup>2+</sup> released from the ER is pumped either back into the ER or out of the cell.

Let  $p$  and  $c$  denote the cytoplasmic concentrations of IP<sub>3</sub> and Ca<sup>2+</sup>, respectively. Then, within each cell the equation for  $p$  is

$$\frac{\partial p}{\partial t} = D_p \nabla^2 p - \frac{V_p p}{k_p + p} \quad (1)$$

where  $D_p$  is the diffusion coefficient of IP<sub>3</sub>,  $\nabla^2 p$  represents the diffusion of IP<sub>3</sub>,  $V_p$  is the maximal rate of IP<sub>3</sub> degradation, and  $k_p$  is the concentration at which IP<sub>3</sub> degradation is half-maximal.

At each cell boundary,

$$D_p \nabla p \cdot \mathbf{n} = F_p (p_+ - p_-) \quad (2)$$

where  $p_+$  and  $p_-$  denote the IP<sub>3</sub> concentrations on either side of the boundary, and  $\mathbf{n}$  is the unit normal vector to the boundary.  $F_p$  is the permeability coefficient, with units of distance/time. Note that, although  $\nabla p$  is continuous across the boundary,  $p$  is not. In our simulations we avoid any problems caused by the orientation of the boundary by solving on a regular grid aligned with the coordinate axes, and defining the cells such that all the cell boundaries are also aligned with the coordinate axes (cf. Fig. 2).

The equations for the Ca<sup>2+</sup> dynamics are slightly more complicated, due to the nature of Ca<sup>2+</sup> release and uptake. As Ca<sup>2+</sup> is released into the cytoplasm through the IP<sub>3</sub> receptor ( $J_{\text{flux}}$ ) or unspecified channels ( $J_{\text{leak}}$ ) and is removed from the cytoplasm by the action of Ca<sup>2+</sup> ATPase pumps ( $J_{\text{pump}}$ ), we have the conservation equation

$$\frac{\partial c}{\partial t} = D_c \nabla^2 c + J_{\text{flux}} = J_{\text{pump}} + J_{\text{leak}} \quad (3)$$

$J_{\text{leak}}$  is assumed to be a constant,

$$J_{\text{leak}} = \beta \quad (4)$$

$J_{\text{pump}}$  is determined from the data of Lytton et al. [16] to be

$$J_{\text{pump}} = \frac{\gamma c^2}{k_\gamma^2 + c^2} \quad (5)$$

To model  $J_{\text{flux}}$  we assume that the IP<sub>3</sub> receptor has four binding sites, one for IP<sub>3</sub> and three for Ca<sup>2+</sup> (one

activating, and two inactivating). Binding of IP<sub>3</sub> opens the receptor, and Ca<sup>2+</sup> binding to the activating site further activates the receptor. Receptor inactivation occurs when Ca<sup>2+</sup> is bound to either of the inactivating binding sites.

The binding of IP<sub>3</sub> and Ca<sup>2+</sup> to the activating site is fast. The binding of Ca<sup>2+</sup> to the inactivating sites is slow. It is assumed that all three different types of binding sites act independently. Thus, if we let  $h$  denote the probability that both of the inactivating sites are unoccupied, we have

$$J_{\text{flux}} = k_f \left( \frac{p}{k_\mu + p} \right) \left( \frac{c}{k_1 + c} \right) h \quad (6)$$

where

$$\tau_h (c + K_4) \frac{dh}{dt} = K_4 K_3 - h(c^2 + K_4 c + K_3 K_4) \quad (7)$$

This equation for  $h$  is derived in Appendix A; it is a generalized form of the original expression of Atri et al. [17].

Due to independence, the open probability of the receptor is the product of the occupation probability of each type of binding site:  $p/(k_\mu + p)$  is the probability IP<sub>3</sub> is bound to the receptor,  $c/(k_1 + c)$  is the probability Ca<sup>2+</sup> is bound to the activating site. Both of these expressions assume simple Michaelis–Menten binding kinetics. The overall form of  $J_{\text{flux}}$  was chosen so as to agree with experimental data from a variety of cell types, including *Xenopus* oocytes, and rat brain synaptosomes. However, to obtain better agreement with the observed responses in glial cells, the steady state open probability curve was shifted slightly to lower Ca<sup>2+</sup> concentrations. Little data is available on the IP<sub>3</sub> receptors of rat brain glial cells, or tracheal epithelium, the two cell types to which the model has been applied. It should be noted that this model cannot reproduce all features of the open probability curve of type I IP<sub>3</sub> receptors observed in lipid bilayers. For instance, recent results of Kaftan et al. [18] show that, as the background IP<sub>3</sub> concentration increases, the peak of the open probability curve of the type I IP<sub>3</sub> receptor shifts to higher calcium concentrations, a feature which is not present in our model. However, a simple theoretical analysis, not given here, shows that the opposite behavior is predicted for type III IP<sub>3</sub> receptors. Since the exact distribution of IP<sub>3</sub> receptor subtypes is not known for our cell types, it is not clear

Table 1

Glossary of model parameters

$k_1 = 0.35 \mu\text{M}$	$k_f = 6 \mu\text{M/s}$
$K_3 = 2.0 \mu\text{M}$	$K_4 = 0.05 \mu\text{M}$
$k\gamma = 0.135 \mu\text{M}$	$k_\mu = 0.1 \mu\text{M}$
$k_p = 1 \mu\text{M}$	$V_p = 0.04 \mu\text{M/s}$
$\gamma = 0.75 \mu\text{M/s}$	$\beta = 0.00375 \mu\text{M/s}$
$\tau_h = 1 \text{ s}$	$D_p = 300 \mu\text{m}^2/\text{s}$
$D_c = 20 \mu\text{m}^2/\text{s}$	$F_p = 1 \mu\text{M/s}$

$k_1$ ,  $K_3$  and  $K_4$  were chosen so as to obtain the correct steady state open probability of the IP<sub>3</sub> receptor, as measured in *Xenopus* oocytes (Parys et al. [21]; Atri et al. [17]).  $\gamma$  and  $\beta$  were chosen to give physiologically reasonable resting Ca<sup>2+</sup> concentrations, and  $V_p$ ,  $k_p$  and  $k_\mu$ , were taken from Sneyd et al. [15].  $D_p$  and  $D_c$  were taken from Allbritton et al. [22].  $k_f$  is just a scaling factor. The value for  $\tau_h$  was chosen between the values used by Atri et al. [17] and Sneyd et al. [15], while the value for  $F_p$  is based on the previous modeling work of Sneyd et al. [15].

what changes should be made to the model to incorporate this shift of the open probability curve. Preliminary computations with other models indicate that this shifting of the open probability curve has no effect on the model predictions presented here.

At each cell boundary,

$$D_c \nabla c \cdot \mathbf{n} = F_c (c_+ - c_-) \quad (8)$$

where, as before,  $c_+$  and  $c_-$  denote the Ca<sup>2+</sup> concentrations on either side of the boundary, and  $\mathbf{n}$  is the unit normal vector to the boundary.  $F_c$  is the permeability coefficient for Ca<sup>2+</sup>.

Mechanical stimulation

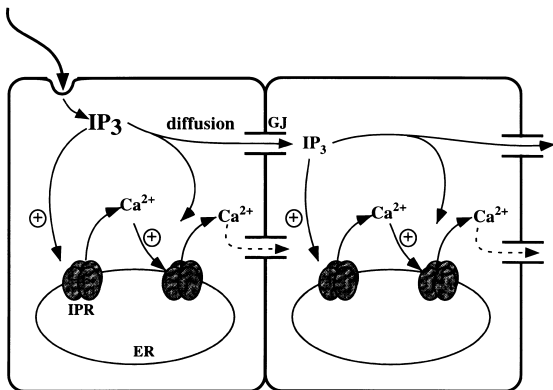


Fig. 1. Schematic diagram of the passive diffusion hypothesis for the propagation of intercellular Ca<sup>2+</sup> waves. IPR, IP<sub>3</sub> receptor/Ca<sup>2+</sup> channel; ER, endoplasmic reticulum; GJ, gap junction. The + sign denotes Ca<sup>2+</sup>-induced Ca<sup>2+</sup> release.

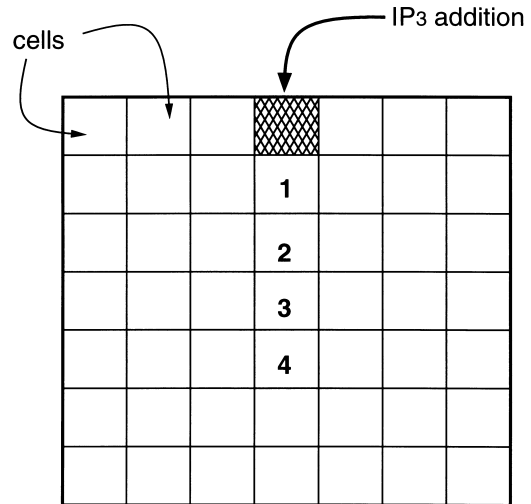


Fig. 2. Diagram of the grid upon which the numerical simulations were performed. Each cell was  $24 \mu\text{m} \times 24 \mu\text{m}$ . The boundary conditions around the edge of the grid were no-flux. Numbers represent cells analyzed in subsequent figures.

Values for the model parameters are given in Table 1.

### 2.1. Numerical methods

The model equations were solved by the Douglas–Rachford ADI algorithm on a grid of  $7 \times 7$  cells, each containing  $16 \times 16$  gridpoints. Since each cell is approximately  $15\text{--}25 \mu\text{m}$  in diameter, this discretization corresponds to about two grid points for every  $3 \mu\text{m}$ .

Simulations with more grid points in each cell showed no significant differences from the results given here (computations not shown). Initially,  $c$  and  $h$  were set to their steady state values corresponding to  $p = 0$ . To simulate a mechanical stimulation IP<sub>3</sub> was added at a rate of  $1 \mu\text{M/s}$  for the first 15 s, to the shaded cell in Fig. 2.

## 3. Results

### 3.1. Spatially-independent oscillations

If the IP<sub>3</sub> concentration is steadily increased in all cells, a situation that precludes the diffusion of IP<sub>3</sub> or Ca<sup>2+</sup> between cells, each model cell will exhibit Ca<sup>2+</sup> oscillations but only within a specific physiological

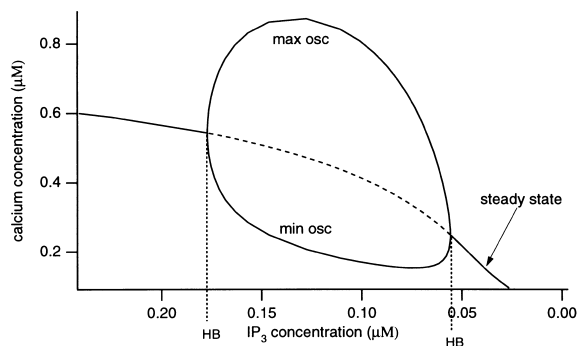


Fig. 3. Bifurcation diagram of a model cell (in the absence of diffusion of  $p$  or  $c$ ). Stable steady states are denoted by solid lines, and unstable ones by dashed lines. At the points labeled HB, the steady state changes stability in a Hopf bifurcation, leading to the existence of a branch of stable limit cycles. Note that  $\text{Ca}^{2+}$  oscillations occur only for an intermediate range of  $\text{IP}_3$  concentrations.

range of  $\text{IP}_3$  concentrations (Fig. 3). Treating  $p$  as a bifurcation parameter, a branch of stable limit cycles appears via a supercritical Hopf bifurcation at  $P = 0.06 \mu\text{M}$  and disappears at a supercritical Hopf

bifurcation at  $P = 0.18 \mu\text{M}$ . In other words, intracellular  $\text{Ca}^{2+}$  oscillations exist only when  $[\text{IP}_3]$  is between 0.06 and 0.18  $\mu\text{M}$ . The importance of this fact will be apparent later.

### 3.2. The intercellular diffusion of calcium

To evaluate the role of intercellular  $\text{Ca}^{2+}$  diffusion on the  $\text{Ca}^{2+}$  waves and subsequent  $\text{Ca}^{2+}$  oscillations, we performed four simulations with different values of  $F_c$ , the intercellular calcium permeability (Fig. 4). The  $[\text{Ca}^{2+}]$ , measured at the middle grid point of the indicated cell (cf. Fig. 2), is plotted as a function of time from three cells. The mechanical stimulation was initiated at time 0. When  $F_c = 0 \mu\text{m/s}$  the  $\text{Ca}^{2+}$  oscillations induced by the  $\text{Ca}^{2+}$  wave remain asynchronous, and show no phase locking. These features are preserved when  $F_c = 0.1 \mu\text{m/s}$ . However, when  $F_c = 1 \mu\text{m/s}$ , the  $\text{Ca}^{2+}$  oscillations begin to become synchronized just prior to the time at which the  $\text{Ca}^{2+}$  oscillations start to subside. When  $F_c = 10$ , the  $\text{Ca}^{2+}$  oscillations of each cell become synchronized quick-

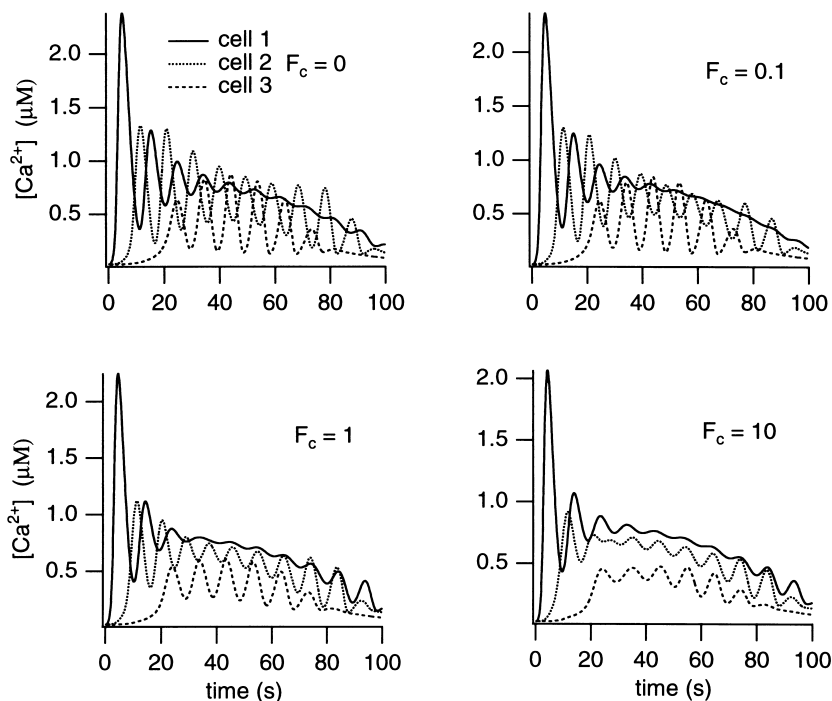


Fig. 4. Synchronization of intracellular  $\text{Ca}^{2+}$  oscillations by intercellular  $\text{Ca}^{2+}$  diffusion. In each panel, the first peak of each trace corresponds to the intercellular wave. When  $F_c$  is high, the intracellular oscillations after the wave quickly synchronize. Since this is not observed experimentally, we conclude that  $F_c$  must be between 0.1 and 1  $\mu\text{m/s}$ .

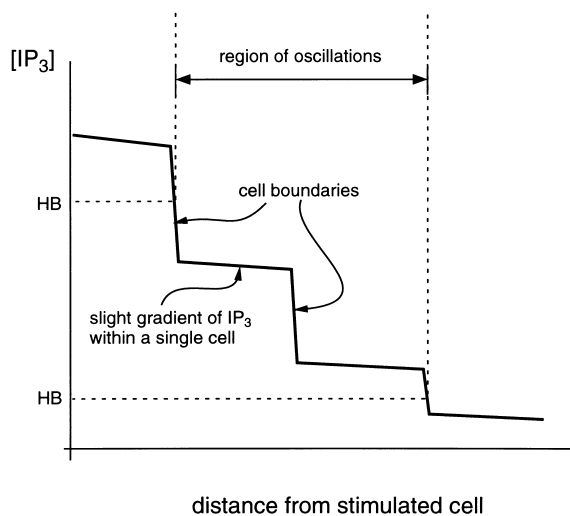


Fig. 5. Schematic diagram (not to scale) of the spatial gradient of  $IP_3$  set up by the mechanical stimulation. Since oscillations occur only when  $[IP_3]$  is in an intermediate range, it follows that oscillations will be seen only in a band a certain distance from the stimulated cell. HB denotes the position of the Hopf bifurcations shown in Fig. 3.

ly. However, experimental data does not show signs of synchrony between neighboring cells [19, Strahonja and Sanderson, unpublished data]. Consequently, it follows that  $F_c$  must be less than  $1 \mu\text{m/s}$ , and probably closer to  $0.1 \mu\text{m/s}$ . This estimate agrees well with a previous estimate of  $0.1 \mu\text{m/s}$  obtained by measuring  $Ca^{2+}$  wave speeds in the intact liver [14].

When  $F_c = 0.1 \mu\text{m/s}$ , diffusion of  $Ca^{2+}$  also has almost no effect on the properties of the intercellular wave (computations not shown). Therefore, we conclude that intercellular  $Ca^{2+}$  diffusion is not likely to be a significant modulator of intercellular  $Ca^{2+}$  waves. This prediction is unaffected by the intercellular permeability to  $IP_3$ , as the model assumes that the intracellular oscillations are coupled by the diffusion of  $Ca^{2+}$ , not  $IP_3$ , between cells. This is because  $Ca^{2+}$  oscillations occur at a constant level of  $IP_3$ ; for instance, when  $F_p = \infty$  and  $F_c = 0$  the intracellular oscillations are uncoupled. It follows that the coupling of intracellular  $Ca^{2+}$  oscillations occurs by a different mechanism than that causing the intercellular wave.

### 3.3. The spatial gradient of $IP_3$

The passive diffusion hypothesis predicts that a

mechanical stimulation sets up a spatial gradient of  $IP_3$  across the culture. Since  $Ca^{2+}$  oscillations occur only when  $[IP_3]$  is between the two Hopf bifurcation points (labeled HB in Fig. 3), the gradient of  $IP_3$ , established by the mechanical stimulation, predicts that intracellular  $Ca^{2+}$  oscillations will occur in a zone of cells at a specific distance from the stimulated cell, as illustrated schematically in Fig. 5. This prediction was confirmed by the experimental data (Fig. 6). Furthermore, the  $IP_3$  gradient predicts that cells closer to the stimulated cell will show a different oscillatory pattern than cells further from the stimulated cell.

According to the model (Fig. 7), the cell closest to the stimulated cell (cell 1) will show some initial

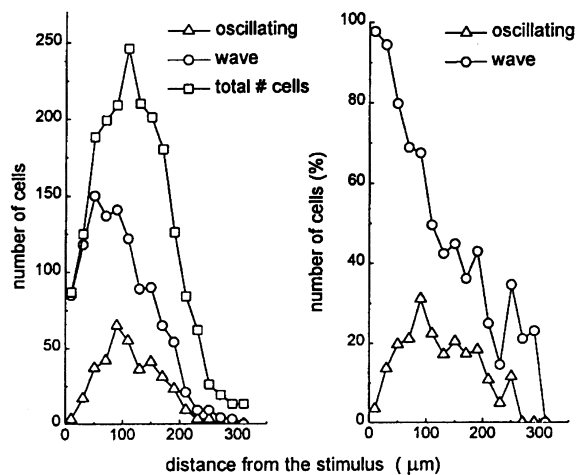


Fig. 6. Experimental data, showing how  $Ca^{2+}$  oscillations induced by a  $Ca^{2+}$  wave occur mostly in a zone around the stimulated cell. The data was collected from mixed glial cell cultures; full details are given in Strahonja and Sanderson (unpublished data). Primary cultures of mixed glial cells were prepared from the brains of 1–2-day-old rat pups, and immunofluorescence staining for cell specific markers was performed to quantify the different cell types in the culture. Mechanical stimulation of a single cell was performed by distorting the cell surface with a micropipette attached to a piezoelectric element, as described in Charles et al. [19]. Cultured cells were loaded with the  $Ca^{2+}$ -sensitive dye fura-2, and the calcium fluorescence was recorded on an optical memory disc recorder for later analysis. The left panel shows the number of cells that exhibit an intercellular wave, that oscillate after the wave, and the total number of cells, all as a function of distance from the stimulated cell. The right panel shows the same data, but this time the numbers of cells that exhibit a wave or that oscillate are expressed as percentages of the total number of cells. The data was taken from 35 experiments, in which a total of 1988 cells were analyzed.

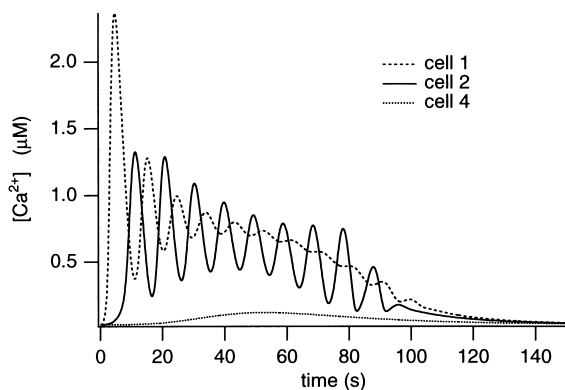


Fig. 7. Response of the model to the addition of  $\text{IP}_3$  to the shaded cell in Fig. 2.  $\text{IP}_3$  was added at  $1 \mu\text{M/s}$  for 15 s, starting at time 0, and the  $\text{Ca}^{2+}$  responses were measured from cells 1, 2 and 4, as indicated by the labels in Fig. 2.

oscillations in  $[\text{Ca}^{2+}]$ , but these oscillations die away leaving  $[\text{Ca}^{2+}]$  at a high level that slowly declines. Cells further away from the stimulated cell (cell 2) will show continuous oscillations, while farther away (cell 4) very little rise in  $[\text{Ca}^{2+}]$  is seen in response to the stimulation. Again, these prediction were confirmed by experimental data (Strahonja and Sanderson, unpublished data). In experiments, a number of oscillatory patterns emerge, one of which is an initial smaller oscillation, followed by a plateau which gradually decreases (Fig. 8); we call this a fast type or F pattern. A second commonly seen oscillatory pattern is one in which the cell exhibits regular oscillations; we call this a continuous type or C pattern. Examination of a number of mechanically-stimulated intercellular waves shows that type F oscillations tend to occur closer to the stimulated cells than do type C oscillations, as is predicted by the model (Strahonja and Sanderson, unpublished data).

Modulation of the spatial gradient of  $\text{IP}_3$  would be predicted to change the oscillatory pattern. This can be achieved by the addition of acetylcholine (ACh) to the culture to produce an approximately uniform rise in  $[\text{IP}_3]$  across the culture. This change in  $\text{IP}_3$  concentration will shift the band of oscillating cells. The model predicts that addition of  $0.3 \mu\text{M}$   $\text{IP}_3$  uniformly across the culture at 40 s after mechanical stimulation changes cell 4 from a non-responsive cell to a C-type oscillator, and changes cell 2 from a C-type oscillator to an F-type (Fig. 9). The change in cell 4 results from the fact that the  $[\text{IP}_3]$  in cell 4 is now large enough to

cause oscillations. Similarly, the  $[\text{IP}_3]$  in cell 2 has become too large to support oscillations (the upper Hopf bifurcation point is crossed.) Again, these predictions are confirmed by experimentation (Fig. 10).

Another example of how modulation of the  $\text{IP}_3$  gradient can change the oscillatory properties can be seen when a background concentration of  $0.05 \mu\text{M}$   $\text{IP}_3$  is added to the model before mechanical stimulation. In this case, the band of C-type oscillations moves further away from the stimulated cell. As can be seen from Fig. 11, addition of background  $\text{IP}_3$  turns cell 4 into a C-type oscillator, while cell 2 behaves in a manner intermediate between an F-type and a C-type oscillator. In addition, the oscillations occur later in the presence of a background  $\text{IP}_3$  concentration.

### 3.4. F-type oscillations

An intuitive prediction of the passive diffusion hypothesis is that if F-type oscillations occur when the  $[\text{IP}_3]$  gets too high, C-type oscillations should occur as the  $[\text{IP}_3]$  decreases to lower values. Surprisingly, F-type oscillations followed by C-type oscillations were not observed in either experiments or model simulations. One explanation for this apparent contradiction is that the dynamic nature of the decrease in  $[\text{IP}_3]$  prevents the establishment of  $\text{Ca}^{2+}$  oscillations (i.e.  $[\text{IP}_3]$  is changing too fast).

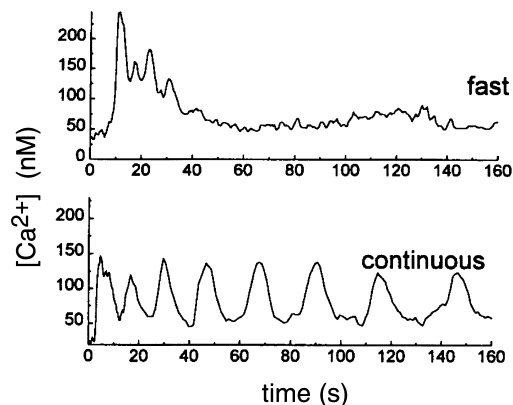


Fig. 8. Experimental data from mixed glial cell cultures, showing two typical responses. Closer to the stimulated cell, the response tends to show an initial oscillatory period, followed by a long plateau which slowly declines (upper panel). A similar response is seen in cell 1 in the numerical simulations (cf. Fig. 7). Further from the stimulated cell, the response is more like a continuous oscillation, as is seen in cell 2 in the model (lower panel). Data taken from Strahonja and Sanderson, unpublished data.

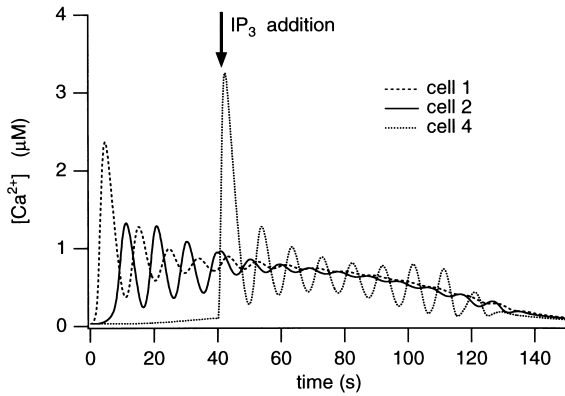


Fig. 9. Model simulations, showing the response to an addition of  $IP_3$ , 40 s after a mechanical stimulation. Cell 4 becomes oscillatory, while the oscillations in cell 2 disappear.

Since this feature is insensitive to noise (as it occurs in experiment also) it is unlikely that it can be explained by the work of Baer et al. [20], who studied the delayed onset of oscillations after passage through a Hopf bifurcation. However, further investigation is needed to confirm this aspect of the hypothesis.

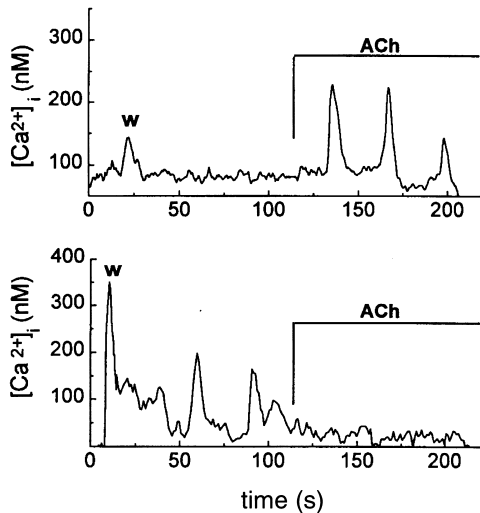


Fig. 10. Experimental data from mixed glial cell cultures, showing the responses to addition of ACh after a mechanical stimulation. Further from the stimulated cell, the ACh tends to initiate oscillations (upper panel), while, closer to the stimulated cell, the ACh tends to eliminate oscillations (lower panel), as predicted by the model results presented in Fig. 9. Data taken from Strallonja and Sanderson, unpublished data.

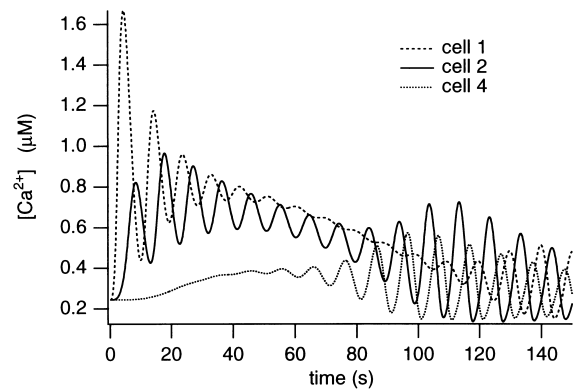


Fig. 11. Model simulations of a mechanical stimulation in the presence of a background  $IP_3$  concentration of  $0.05 \mu M$ . Oscillations occur in cell 4, but at a later time, while the behavior of cell 2 is intermediate between F-type and C-type oscillations.

#### 4. Conclusions

A mathematical model, describing the passive diffusive hypothesis for intercellular  $Ca^{2+}$  signaling is presented. Previous work demonstrated that this model accurately predicted the experimental  $Ca^{2+}$  wave parameters of arrival time and intercellular delay as well as the peak  $Ca^{2+}$  concentrations achieved [15]. Here we demonstrate, by comparison with experimental data, that this same model accurately predicts (a) that  $Ca^{2+}$  oscillations induced by a  $Ca^{2+}$  wave occur in a cellular zone at a specific distance from the stimulated cell, and (b) that the position of this zone is dependent on the background  $IP_3$ . In addition, the model predicts that with an intercellular  $Ca^{2+}$  permeability in the order of  $0.1 \mu m/s$  the intercellular diffusion of  $Ca^{2+}$  is not a major modulator of the intercellular wave.

#### Acknowledgements

This work was supported by NIH grant HL49288 to

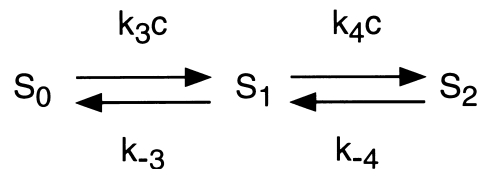


Fig. 12. Binding diagram of the inactivation binding site of the  $IP_3$  receptor.

MJS and NSF grant DMS-9706565 and NIH grant R01 GM56126 to JS. MW was supported by the Marsden Fund of the Royal Society of New Zealand, and by the University of Canterbury, New Zealand.

### Appendix A Derivation of the equation for $h$

We assume that the  $IP_3$  receptor must bind two  $Ca^{2+}$  ions to be inactivated; the binding diagram of the inactivation site is given in Fig. 12. Assuming mass action kinetics, we get

$$\frac{dS_1}{dt} = k_3 c S_0 - k_3 S_1 + k_{-4} S_2 - k_4 c S_1 \quad (9)$$

$$\frac{dS_2}{dt} = -k_{-4} S_2 + k_4 c S_1 \quad (10)$$

Due to the law of conservation,  $S_0 + S_1 + S_2 = 1$  the equation for  $S_0$  is not needed. Assuming that binding of the second inactivating  $Ca^{2+}$  is much faster than binding of the first (and thus the receptor shows extreme positive cooperativity), we get the quasi-steady state relation  $c S_1 = K_4 S_2$ , where  $K_4 = k_{-4}/k_4$ . Hence, letting  $h = S_0$ , we get

$$\tau_h (c + K_4) \frac{dh}{dt} = k_3 k_4 - h (c^2 + K_4 c + K_3 K_4) \quad (11)$$

where  $K_3 = k_{-3}/k_3$  and  $\tau_h = 1/k_3$ .

### References

- [1] M.J. Sanderson, A.C. Charles, S. Boitano, E.R. Dirksen, Mol. Cell. Endocrinol. 98 (1994) 173.
- [2] M.J. Sanderson, News Physiol. Sci. 11 (1996) 262.
- [3] L. Moore, M.J. Sanderson, J. Cell Sci. (1997) in press.
- [4] L. Leybaert, K. Paemeleire, A. Strahonja, M.J. Sanderson (1997) in press.
- [5] A.C. Charles, Dev. Neurosci. 16 (1994) 196.
- [6] M. Nedergaard, Science 263 (1994) 1768.
- [7] J.W. Dani, S.J. Smith, Ciba Found. Symp. 188 (1995) 195.
- [8] M.H. Nathanson, A.D. Burgstahler, A. Mennone, M.B. Fallon, C.B. Gonzalez, J.C. Saez, Am. J. Physiol. 269 (1995) G167.
- [9] L.D. Robb-Gaspers, A.P. Thomas, J. Biol. Chem. 270 (1995) 8102.
- [10] D.E. Clapham, J. Sneyd, Adv. Second Messenger Phosphoprotein Res. 30 (1995) 1.
- [11] Y. Osipchuk, M. Cahalan, Nature 359 (1992) 241.
- [12] T.D. Hassinger, P.B. Guthrie, P.B. Atkinson, M.V. Bennett, S.B. Kater, Proc. Natl. Acad. Sci. USA 93 (1996) 13268.
- [13] M.K. Frame, A.W. de Feijter, Exp. Cell Res. 230 (1997) 197.
- [14] M. Wilkins, J. Sneyd, J. Theor. Biol. (1998) in press.
- [15] J. Sneyd, B. Wetton, A.C. Charles, M.J. Sanderson, Am. J. Physiol. (Cell Physiol.) 268 (1995) C1537.
- [16] J. Lytton, M. Westlin, S.E. Burk, G.E. Shull, D.H. MacLennan, J. Biol. Chem. 267 (1992) 14483.
- [17] A. Atri, J. Amundson, D. Clapham, J. Sneyd, Biophys. J. 65 (1993) 1727.
- [18] E.J. Kaftan, B.E. Ehrlich, J. Watras, J. Gen. Physiol. 110 (1997) 529.
- [19] A.C. Charles, J.E. Merrill, E.R. Dirksen, M.J. Sanderson, Neuron 6 (1991) 983.
- [20] S. Baer, T. Erneux, J. Rirlzel, SIAM J. Appl. Math. 49 (1989) 55.
- [21] J.B. Parys, S.W. Sernett, S. DeLisle, P.M. Snyder, M.J. Welsh, K.P. Campbell, J. Biol. Chem. 267 (1992) 18776.
- [22] N.L. Allbritton, T. Meyer, L. Stryer, Science 258 (1992) 1812.